Antenna Measurement on Cylindrical Surface in Fresnel Region Using Direct Far-Field Measurement System

Soon-Soo Oh, Joung-Myoun Kim, and Jaehoon Yun

The small anechoic chambers built by many small-/medium-sized companies and universities present difficulties in testing electrically large antennas because the chamber size cannot satisfy the far-field criterion of large antennas. In this paper, a method for Fresnel-region measurement on a cylindrical surface with variation of the measurement height is proposed and verified by both calculations and experiments. We implement the proposed method using a direct far-field measurement system by adding a few supporting structures. The results show good accuracy.

Keywords: Antenna measurement, Fresnel region, far-field measurement.

Manuscript received Aug. 11, 2006; revised Nov. 15, 2006.

Soon-Soo Oh (phone: + 82 42 860 4974, email: ssoh@etri.re.kr), Joung-Myoun Kim (email: kjmin@etri.re.kr), and Jaehoon Yun (email: jhyun@etri.re.kr) are with Radio & Broadcasting Research Division, ETRI, Daejeon, Korea.

I. Introduction

Although the border between the far-field and near-field has not been definitively agreed upon [1], the far-field region, or far zone, has usually been referred to as the distance $D_{far} \geq 2L^2/\lambda$, where D_{far} is the distance between the source antenna and probe antenna, L is the aperture diameter, and λ is the free-space wavelength [2]-[4]. The near-field region is the inner area of the far zone. It can be classified into the reactive and radiating near fields [3], [4]. Both near-field scanning measurement and Fresnel-region measurement are related to the radiating near-field region. Near-field scanning is usually performed between 3λ and 10λ, and the Fresnel-region method is usually performed between $\sqrt{(L^3/16\lambda)}$ and $2L^2/\lambda$ [5].

The exact far-field pattern can be obtained by satisfying the criterion, $D_{far} \geq 2L^2/\lambda$. For example, the far-field distance of an antenna of $L = 20\lambda$ operating at 10 GHz is 24 m. Although the aperture dimension is not too large as the subarray shown in [6], the most popular small anechoic chamber occasionally could not measure the far-field pattern because of its small size.

To overcome this problem, an outdoor far-field measurement system can be developed, but it has low security and is sensitive to the weather or moisture. One option is to build a compact range chamber reducing the distance and expanding the quiet zone [7]. A second option is to purchase a near-field scanning system. However, these systems are very expensive, so they are too much of a financial burden for small or medium-sized companies and universities.

Recently, a method utilizing data from several cut-planes in the Fresnel region has been studied [2], [5], [8]-[10]. The cut-

planes are achieved by changing the antenna under test (AUT) elevation angle. Some direct far-field measurement system can adopt this method, so that an expensive near-field measurement system does not need to be purchased. In addition to the advantage of the low cost as compared to the near-field scanning method, this Fresnel-region method can reduce the measurement time because the required scanning planes are smaller, and near-field to far-field transformations are unnecessary.

During Fresnel-region measurement using the method proposed in [5], the AUT should be inclined forward, or leaned backward. This technique, however, creates safety issues because the weight of a large antenna could be several tens of kilograms. Furthermore, the antenna looks down to the lower walls or looks up to the upper walls of the anechoic chamber; therefore, the reflected waves from the lower and upper walls are more detected.

In this paper, a modified Fresnel-region measurement method is proposed. The antenna simply moves downward or upward; therefore, the necessary cost is low or even negligible in some systems. This paper is organized as follows. In section II, the theory and procedure of the measurement are discussed in detail. Section III shows the radiation pattern and gain from calculation and measurement. Conclusions are given in section IV.

II. Measurement Theory and Procedure

1. Principle

The principle of Fresnel-region measurement is illustrated in Fig. 1. An antenna at the origin radiates an electromagnetic wave, and some waves arrive in the blue-shaded area in the Fresnel region, as shown in Fig. 1. This area acts as another source and radiates a wave toward the far-field region [11]. Therefore, the field in the far zone can be said to be formed by the field in the Fresnel region. The strongest contributor is the data on the straight line to the antenna, and the other data contributes by its weighting factor. Therefore, far-field region data can be obtained by multiplying the Fresnel-region data by the weighting factor, and, then, summing these data [2], [5], [8]-[10].

2. Angle Variation Method

The angular coordinate used in this paper is shown in Fig. 2. The shaded area is the antenna aperture, L_x and L_y are the lateral length of the aperture in the x- and y-directions, α is the angle from the y-z plane, and β is the angle from the x-z plane. From our derivation, simulation, and experiment, some indices of the exponential functions in [5] were thought to be

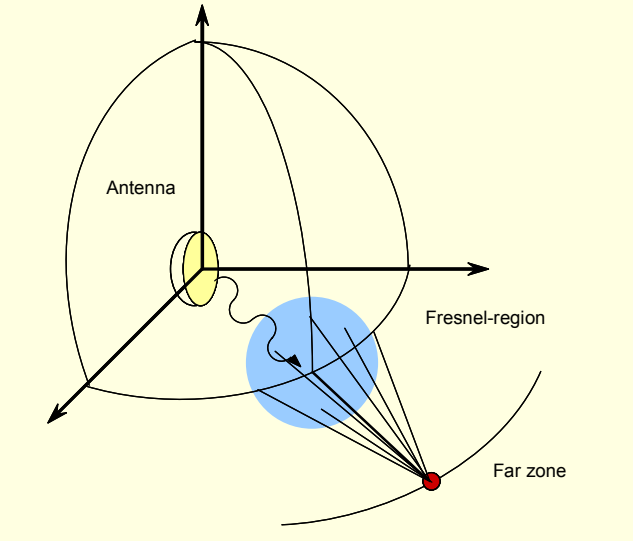

Fig. 1. Principle of Fresnel-region measurement.

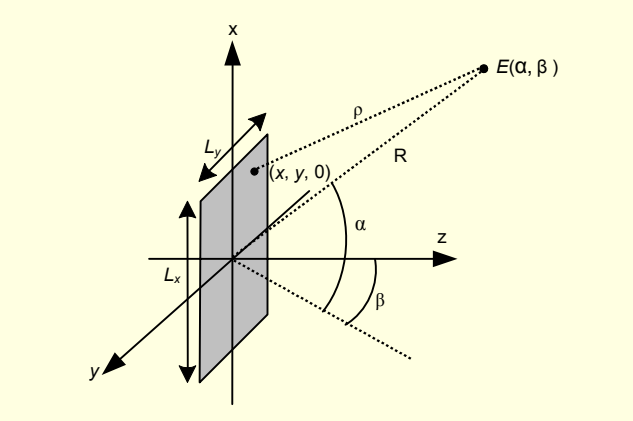

Fig. 2. Angular coordinate.

wrong; therefore, all the equations are derived again in this section.

The E-field pattern of the distance R in the Fresnel region is

$$E_R(\alpha,\beta) = \iint_S h(x,y) e^{-i\frac{2\pi}{\lambda}\rho} dxdy \,, \qquad (1)$$

where

$$\rho = \sqrt{(R\sin\alpha - x)^2 + (R\cos\alpha\sin\beta - y)^2 + (R\cos\alpha\cos\beta - 0)^2}\,.$$

Applying the binomial expression and assuming small α and β, ρ can be written as

$$\rho = R - (x\sin\alpha + y\cos\alpha\sin\beta) + \frac{x^2\cos^2\alpha + y^2\cos^2\beta}{2R}. \qquad (2)$$

Substituting (2) into (1) and applying $f(x,y) = h(x,y)e^{-j2\pi\lambda/R}$,

Fresnel field E_R becomes

$$E_R(\alpha,\beta) = \iint_S h(x,y) e^{-j\frac{2\pi}{\lambda}R} e^{+i\cdot\frac{2\pi}{\lambda}(x\cdot\sin\alpha + y\sin\beta\cos\alpha)} \cdot e^{-i\cdot\frac{\pi}{\lambda R}(x^2\cdot\cos^2\alpha + y^2\cos^2\beta)} dxdy = \iint_S f(x,y) e^{+i\cdot\frac{2\pi}{\lambda}(x\cdot\sin\alpha + y\sin\beta\cos\alpha)} e^{-i\cdot\frac{\pi}{\lambda R}(x^2\cos^2\alpha + y^2\cos^2\beta)} dxdy. \quad (3)$$

With the far-field approximations of $x^2/R \approx 0$ and $y^2/R \approx 0$ due to large R, E-field pattern in the far-zone is reduced to

$$E_{far}(\alpha,\beta) = \iint_S f(x,y) e^{+i\cdot\frac{2\pi}{\lambda}(x\cdot\sin\alpha + y\sin\beta\cos\alpha)} dxdy\,. \quad (4)$$

In order to find the relation between (3) and (4), the Fourier series (5) can be used:

$$e^{+i\cdot\frac{\pi}{\lambda R}(x^2\cos^2\alpha + y^2\cos^2\beta)} = \sum_{m=-\infty}^{+\infty}\sum_{n=-\infty}^{+\infty} k_{mn} e^{+j\frac{2\pi}{L_x}mx} e^{+j\frac{2\pi}{L_y}nx}, \quad (5)$$

where Fourier coefficient k_{mn} is

$$k_{mn} = \frac{1}{L_x L_y}\int_{-L_x/2}^{L_x/2} e^{+ic^2u^2} e^{-i\frac{2\pi}{L_x}mu} du \int_{-L_y/2}^{L_y/2} e^{+ic^2v^2} e^{-i\frac{2\pi}{L_y}mv} dv, \quad (6)$$

and $c^2 = \pi/(\lambda R)$.

Substituting (5) into (3), and comparing to (4), the relation between the E_{far} and E_R as given in [2], [5], [8] is

$$E_{far}(\alpha,\beta) = \sum_{m=-M}^{+M}\sum_{n=-N}^{+N} k_{mn}\cdot E_R(\alpha + m\Delta\alpha,\ \beta + n\Delta\beta), \quad (7)$$

where $\Delta\alpha = \lambda/L_x$ and $\Delta\beta = \lambda/L_y$.

Equation (7) indicates that E-field in the far-field region is the summation of the product of k_{mn} and several E-fields in the Fresnel region as describe before. The E-fields used in summation are obtained at a finite number of angles, $m\Delta\alpha$ and $n\Delta\beta$. The probing points $m\Delta\alpha$ are shown as red dots in Fig. 3, and $n\Delta\beta$ can be drawn in a similar way to Fig. 3 in the horizontal space. Since only the angle of the probing position changes, we named this technique the angle variation method to prevent confusion in comparison to the height variation method proposed in this paper.

The angle variation method can be carried out by inclining the positioner of the probe or source antenna; therefore, there could be a safety and error problem. Some measurement systems cannot incline the positioner.

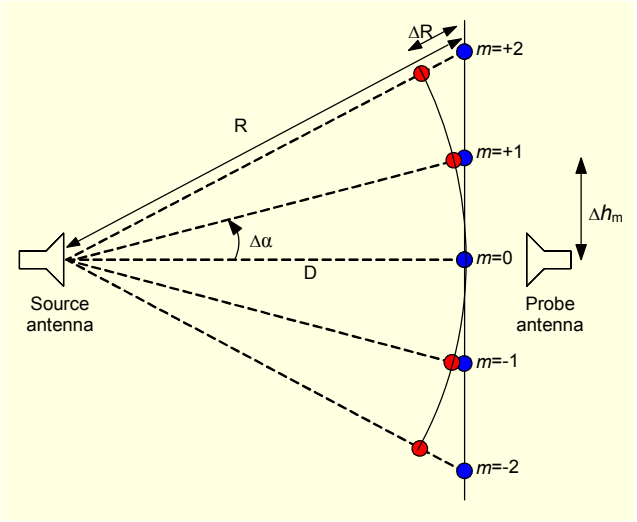

Fig. 3. Scheme of Fresnel-region measurement. Red points represent the angle variation method, and blue points reprensent the proposed height variation method.

3. Height Variation Method

The proposed Fresnel-region measurement method, or height variation method, is illustrated in Fig. 3. Electric fields measured at the blue points are transformed into electric fields at the red points. The probe antenna moves in the vertical direction and then rotates centering on the source antenna in the horizontal direction. In other words, the probe antenna moves on the cylindrical surface, measuring the electric fields.

Equation (7) can be re-organized as

$$E_{far}(\alpha,\beta) = \sum_{m=-M}^{+M}\sum_{n=-N}^{+N} k_{mn}\cdot\{E_D(\alpha + m\Delta\alpha, \beta + n\Delta\beta)\cdot C_{m,S}\cdot C_{m,R}\}, \quad (8)$$

where E_R is the electric field at distance R as shown in Fig. 3, and $C_{m,S}$ and $C_{m,R}$ are the compensating coefficients.

The coefficient $C_{m,S}$ compensates for the imperfect source antenna pattern because the magnitudes and phases at an off-boresight angle of the source antenna deviate from those at a boresight angle. The magnitude and phase of $C_{m,S}$ can be easily obtained by measuring the source antenna. Then, the magnitude is normalized and multiplied after being inversed, and the phase is subtracted.

Since $C_{m,S}$ depends on the measurement distance R, the measurement of the source antenna should be performed at the same distance as that at which the Fresnel-region measurement will be performed. The coefficient $C_{m,S}$ is also dependent on the aperture size of the source antenna. A large aperture of the source antenna results in a large variation of $C_{m,S}$ over the azimuth angle. On the other hand, a source antenna with a

small aperture, for example, an open-ended waveguide, has a broad beamwidth and, thus, little variation of $C_{m,S}$ versus the azimuth angle. From our simulations and experiments, the compensating term $C_{m,S}$ of the small-aperture source antenna has almost no effect on the gain and radiation pattern.

The coefficient $C_{m,R}$ is also the compensating term of

$$C_{m,R} = (1 + \Delta R/(R - \Delta R)) \angle (k\Delta R), \quad (9)$$

where k is the wave number. Since the differential distance between R and D is ΔR as drawn in Fig. 3, the magnitude and phase are compensated by ΔR. The compensating term $C_{m,R}$ is irrelevant to the antenna size and only relevant to the physical and electrical distance as written in (9). If distance R is large enough, $\Delta R/R$ can be negligible; thus, the coefficient $C_{m,R}$ becomes a function of phase $k\Delta R$.

It must be noted that (9) is an approximation and is only valid for an electrically large antenna having a narrow beamwidth. For an antenna with a small aperture, the required number of cut planes, m, the angle $\Delta\alpha \times |m|$, and the differential distance ΔR also increase. The relatively large ΔR must result in a large error while compensating it by (9). In this case, a more complicated compensating technique should be developed.

The required height variation can easily be calculated from Fig. 2 as

$$\Delta h_m = D \times \tan(\Delta\alpha \times |m|). \quad (10)$$

The minimums of M and N in (7), $M_{\min}$ and $N_{\min}$, were suggested in [5], but from some of our calculations and experiments, those numbers, $M_{\min}$ and $N_{\min}$ were inaccurate for the relatively small but still large antenna. For this reason, a simpler approach has been utilized in this study which is similar to that in [9].

As shown in Fig. 4, $|k_{mn}|$, the normalized magnitude of k_{mn}, decreases as the index of m or n increases. For example, $|k_{mn}|$ is about -18 dB at $m, n = \pm 4$. This very small amount of k_{mn} does not contribute much to the summation in (7) and can be ignored. From this fact, we can determine the required m and n from the plot of the normalized magnitude of k_{mn}. Our empirical criterion is that $|k_{mn}|$ should drop by more than 15 dB from the highest $|k_{mn}|$.

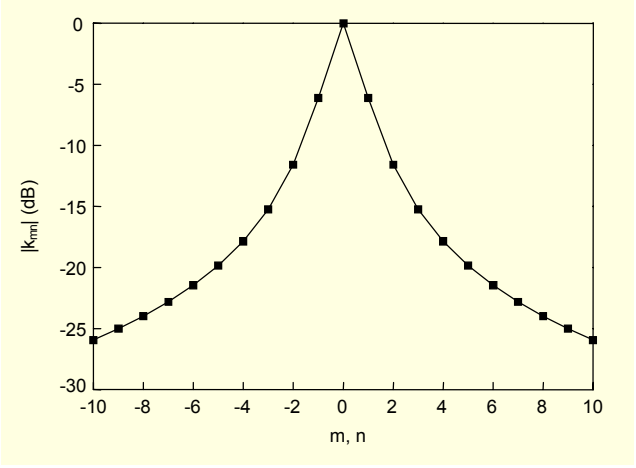

Fig. 4. Normalized k_{mn}, $|k_{mn}|$ for m, n. $L_x = L_y = 5\lambda$, $R = 16.7\lambda$.

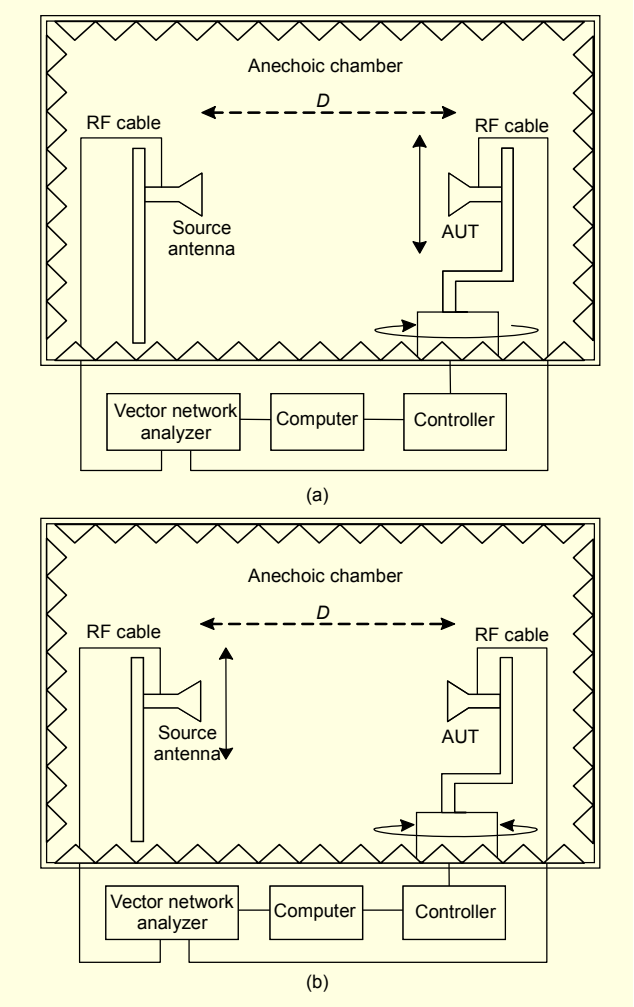

Fig. 5. Configuration examples of Fresnel-region measurement system.

4. Procedure of Measurement and Data Acquisition

Possible configurations of the Fresnel-region measurement system are illustrated in Fig. 5. The source antenna and AUT are separated by distance D, which is the Fresnel-region distance. The source antenna radiates RF power and the AUT receives it. The AUT rotates on its turntable. These configurations are identical to the direct far-field measurement setup. The only difference is that the AUT should be raised or lowered as shown in Fig. 5(a) or the source antenna should be

moved as shown in Fig. 5(b).

Besides these configurations, other systems can be utilized based on the reciprocal theory. The AUT can transmit RF power, or the source antenna can turn around on the azimuth plane.

The procedure of the proposed Fresnel-region measurement is illustrated in Fig. 6. After the parameters are decided based on the equations, the radiation pattern is first measured at the lowest (or highest) height rotating the turntable, and its measured complex data is saved in the database. After the position of the AUT is adjusted upward (downward), this process is repeated until it reaches its highest (lowest).Next, the required complex data E_D is extracted from the database, and k_{mn}, $C_{m,R}$, and $C_{m,S}$ are calculated. Finally, far-field radiation patterns can be obtained from the Fresnel-to-far-field calculation in (8).

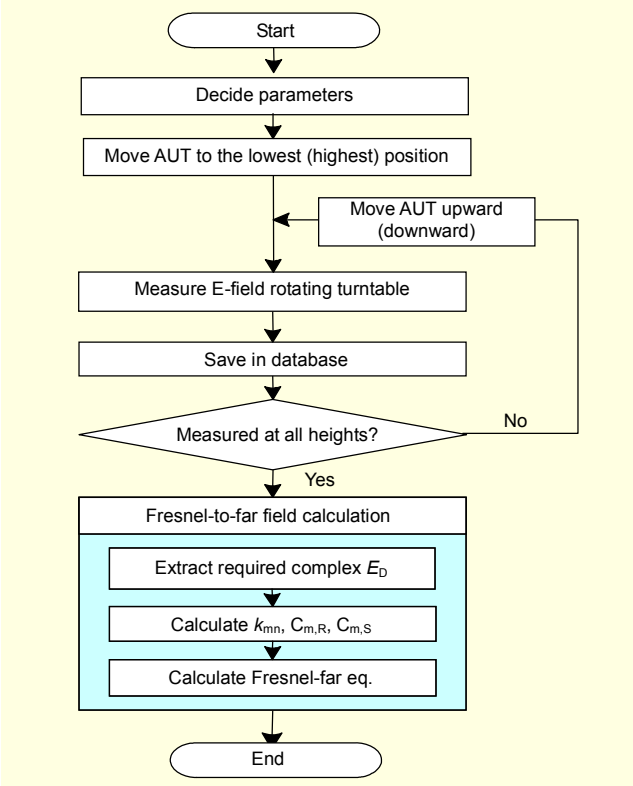

Fig. 6. Procedure of Fresnel-region measurement.

III. Calculation and Measurement Results

1. Calculated Radiation Pattern

The verification of the proposed method was performed for a $5\lambda \times 5\lambda$ square aperture having an ideally uniform current distribution. The frequency was set at 10 GHz. The minimum required far-field distance is 3.0 m, but the method was applied at the reduced distance of 0.5 m (16.7λ).

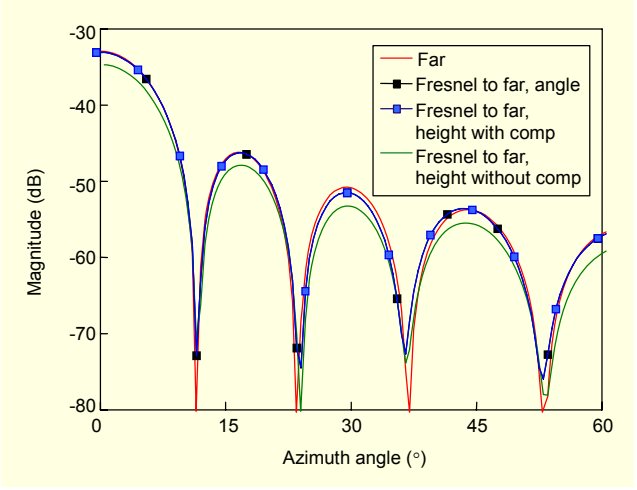

Fig. 7. Radiation patterns of far-field and Fresnel-to-far field calculations. The aperture dimension is $5\lambda \times 5\lambda$ having an ideally uniform current distribution.

Five cut planes were required from the plot of $|k_{mn}|$ as shown in Fig. 4, so that $\Delta\alpha = \Delta\beta = 11.5°$, $\Delta h_m = 0, \pm 0.102$ and ± 0.212 m.

The electric field in the Fresnel region was calculated from (1). The method of angle variation and the proposed height variation method were applied to the Fresnel-field data. The reference far-field pattern was obtained from (4). The E-plane patterns for three cases are plotted in Fig. 7. The transformed pattern of the height variation with compensation shows good agreement with the reference far-field pattern. It also closely matches the radiation pattern using the angle variation method.

In order to investigate the compensation effect of $C_{m,S}$ and $C_{m,R}$, the radiation pattern without compensation parameters was also calculated. Compared to the pattern having compensation, it does not agree with the reference far-field pattern; therefore, it can be said that the compensation parameters, $C_{m,S}$ and $C_{m,R}$ operate very well. It should be noted that a higher number of cut planes results in greater accuracy.

The compensation effect can be clearly observed in Fig. 8. The magnitudes and phases of each cut-plane in the Fresnel region obtained from (1) are compared. Index m is consistent with that in Fig. 3. The red and blue lines represent the electric fields of the red and blue points of Fig. 3. The green curves are the compensated data from the blue curves.

As can be seen in Fig. 8(a), the magnitudes for $m = 1$ are similar to each other because the distance difference ΔR is small; however, those for $m = 2$ are a little different. From Fig. 8(a), it seems that the compensating terms are meaningless. However, as shown in Fig. 8(b), the phases between the angle variation (red line) and height variation (blue line) method are much different. The compensated phases (green line) are

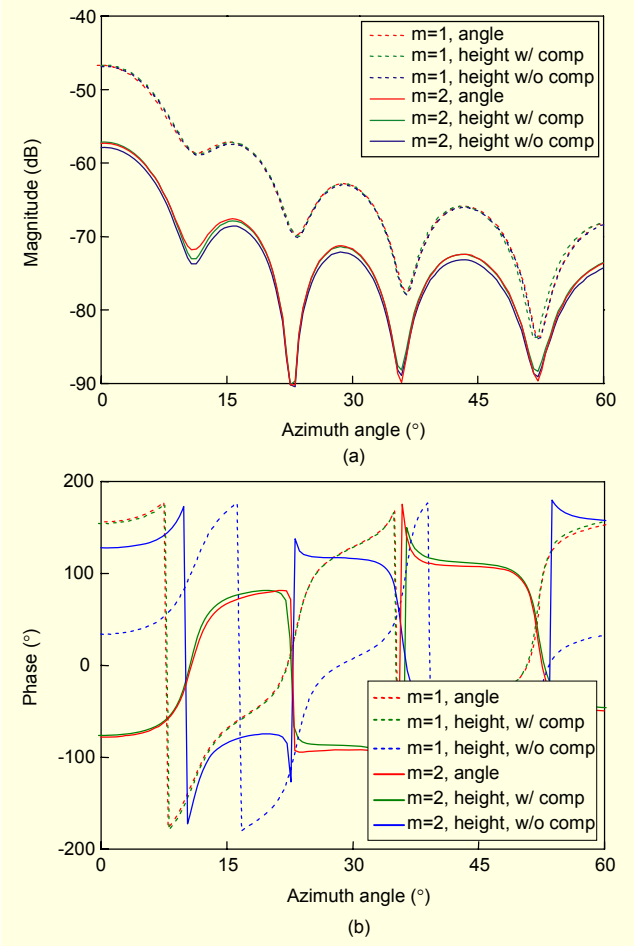

Fig. 8. Magnitudes and phases of Fresnel field for $m = 1, 2$. Angle variation and height variation methods with or without compensation are compared. (a) Magnitude and (b) phase.

almost equal to the phases of the angle variation method for both $m = 1$ and $m = 2$. This demonstrates again that the compensation technique is useful, and the height variation technique can result in accurate radiation pattern and gain.

2. Measured Radiation Pattern

The proposed method in this paper was also verified by experimental data. For the AUT, we adopted the standard horn antenna (model name: SGA-110) shown in Fig. 9. The aperture dimension was 152.4 mm × 108.4 mm. The AUT was measured at 10 GHz. The reference far field and the Fresnel field were measured in different-sized anechoic chambers at ETRI. The reference far-field pattern was measured at 8 m, much further than D_{far} = 2.33 m. The Fresnel field was measured at the distance of 0.5 m with five heights, $\Delta h_m = 0$, ±0.100, and ±0.208 m. Given the aperture dimensions (L_x = 108.4 mm, and L_y = 152.4 mm), $\Delta\alpha$ is 15.9°, and $\Delta\beta$ is 11.3°. As shown in Fig. 9, the near-field scanner was utilized to

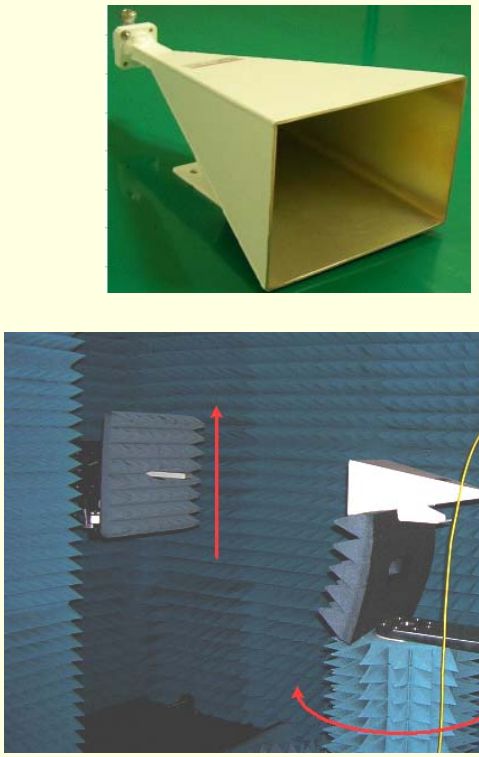

Fig. 9. SGA-110 horn antenna and experimental setup in ETRI anechoic chamber.

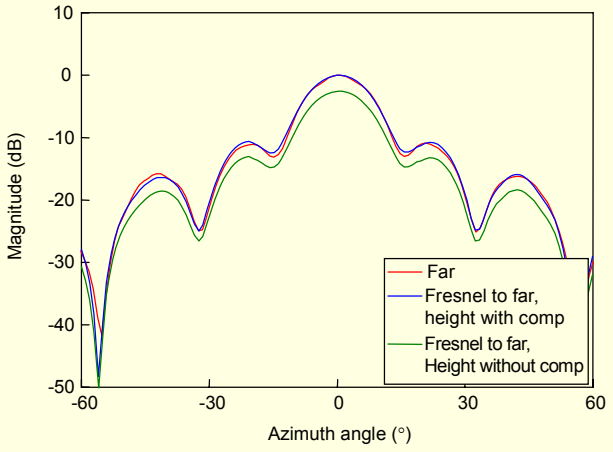

Fig. 10. E-plane pattern of SGA-110 horn antenna.

move the source antenna, and the turntable holding the SGA-110 was rotated.

The E-plane radiation patterns are plotted in Fig. 10. The Fresnel-field to far-field pattern shows good agreement compared to the reference far-field pattern. As with the calculated patterns of Fig. 8, the pattern of the Fresnel-field to far-field transformation without compensation technique strongly disagrees with the exact far-field pattern, particularly

in the peak gain level.

3. Measured Gain

The Fresnel-field to far-field transformation gain, $G_{\text{Fresnel-far}}$ can be obtained from (11), which is called the gain comparison method [3], [5].

$$G_{\text{Fresnel-far}} = G_s + (P_T - P_M), \quad (11)$$

where G_S is the gain of the standard antenna satisfying the far-field condition, P_T is the Fresnel-field to far-field transformed power for AUT, and P_M is the measured power for the standard antenna. We used the FLANN Microwave 17240-10 horn antenna as the standard antenna. Since the aperture dimension of the 17240-10 horn is 28.9 mm × 19.7 mm, the minimum far-field distance is 0.08 mm, which is much less than the distance of the Fresnel-region measurement, 0.5 m.

The power and gain are summarized in Table 1. The gain from the commercial gain-chart of SGA-110, $G_{\text{gain-chart}}$, is also included in Table 1. The transformed gain, $G_{\text{Fresnel-far}}$ is +21.97 dBi, and agrees well with $G_{\text{gain-chart}}$ with a slight difference of 0.36 dB. The gain of 19.41 dBi without the compensation terms is also included in Table 1.

Table 1. Gain from the Fresnel-field to far-field transformation and the commercial gain-chart.

G_S (dBi)	P_T (dB)	P_M (dB)	$G_{\text{Fresnel-far}}$ (w/ comp) (dBi)	$G_{\text{Fresnel-far}}$ (w/o comp) (dBi)	$G_{\text{gain-chart}}$ (dBi)
+8.70	+12.47	-0.80	+21.97	+19.41	+21.61

IV. Conclusion

A method for Fresnel-region measurement on a cylindrical surface with variation of the measurement height was proposed. To verify the proposed method, the radiation pattern of the uniform aperture was calculated, and the results showed good accuracies. Additionally, an experiment using the SGA-110 horn antenna was conducted. The Fresnel-to-far-field transformation radiation pattern and gain were obtained. When compared to the reference data, They showed good agreements. As demonstrated by the configuration examples and test procedure, this method can be easily implemented using a direct far-field measurement system. The only additional requirement is the ability to change the measurement height. The height can be changed manually if the design of the supporting structure for the antenna allows, or it can be changed automatically by the motor.

References

[1] C. Capps, "Near Field or Far Field?" *EDN (Electronic Design News: http://www.edn.com)*, Aug. 2001, pp. 95-102.

[2] G.E. Evans, *Antenna Measurement Techniques*, Artech House, Boston, 1990.

[3] J.D. Kraus and R.J. Marhefka, *Antennas for All Applications*, 3rd Ed., McGraw-Hill, Boston, 2002.

[4] A.W. Rudge, K. Milne, A.D. Olver, and P. Knight, *The Handbook of Antenna Design*, IEE, London, 1986.

[5] I.L. Vilenko, A.A. Meduhin, Y.A. Suserov, A.K. Tobolev, and A.V. Shishlov, "Reconstruction of Antenna Radiation Pattern by Using Data of Measurements in a Fresnel Region with Test Facility Intended for Far-Field Measurements," *Antennas,* Jan. 2005, pp. 46-92 (in Russian).

[6] U.H. Park, H.S Noh, S.H Son, K.H. Lee, and S.I. Jeon, "A Novel Mobile Antenna for Ku-Band Satellite Communications," *ETRI Journal*, vol. 27, no. 3, June 2005, pp. 243-249.

[7] L.H. Hemming, *Electromagnetic Anechoic Chambers: A Fundamental Design and Specification Guide*, John Wiley & Sons, New York, 2002.

[8] G.E. Evans, "Far-Field Correction for Short Antenna Ranges," *Proc. AMTA*, 1985, pp. 34-1–34-9.

[9] K. Wu and S. Parekh, "Method of Transforming Antenna Fresnel Region Fields to Far Region Fields," *Proc. AMTA*, 1989, pp. 11-9–11-14.

[10] K. Wu and S. Parekh, "A Method of Transforming Fresnel Field to Far Field for Circular Aperture Antennas," *IEEE APS-Digest*, May 1990, pp. 216-219.

[11] H.D. Hristov, *Fresnel Zones in Wireless Links, Zone Plate Lenses and Antennas*, Artech House, Boston, 2000.

Soon-Soo Oh received the BS and MS degrees in electronics engineering from Inha University, Incheon, Korea, in 1998 and 2000, respectively, and the PhD degree in radio sciences and engineering, Korea University, Seoul, Korea. From Sept. 2003 to April 2005, he was a Post-Doc Fellow at the Dept. of Electrical and Computer Engineering in University of Manitoba, Canada. Since May 2005, he has been a Senior Member of Research Staff, in the Radio Technology Group of Electronics and Telecommunications Research Institute (ETRI), Korea. His research interests include numerical analysis, antenna design and measurement, and electromagnetic metamaterials.

Joung-Myoun Kim received the BS degree in electronics engineering from Hanbat National University, Daejeon, Korea, in 2004, and the MS degree in electronics engineering from Chungbuk National University, Korea, in 2007. He is currently a member of the Radio Technology Group of ETRI. His research interests include antenna measurement. He is a member of the AMTA (Antenna Measurement Techniques Association).

Jaehoon Yun received the BS, MS, and PhD degrees in electronic engineering from Chungang University, Seoul, Korea, in 1984, 1986, and 1999, respectively. Since 1990, he has been with ETRI, Korea. He is currently a Project Leader of Antenna Measurement System Development, a professor of Korea University of Science & Technology (UST), and an ETRI Journal Editor on RF & broadcasting technology. His work has been in the fields of standard field generation technology, electromagnetic compatibility in the wireless phone, calibration technology of electric and magnetic field probes, and antenna measurement systems.